



A Jurassic ornithischian dinosaur from Siberia with both feathers and scales

Pascal Godefroit *et al.*
Science **345**, 451 (2014);
DOI: 10.1126/science.1253351

This copy is for your personal, non-commercial use only.

If you wish to distribute this article to others, you can order high-quality copies for your colleagues, clients, or customers by [clicking here](#).

Permission to republish or repurpose articles or portions of articles can be obtained by following the guidelines [here](#).

The following resources related to this article are available online at www.sciencemag.org (this information is current as of July 24, 2014):

Updated information and services, including high-resolution figures, can be found in the online version of this article at:

<http://www.sciencemag.org/content/345/6195/451.full.html>

Supporting Online Material can be found at:

<http://www.sciencemag.org/content/suppl/2014/07/23/345.6195.451.DC1.html>

This article **cites 42 articles**, 5 of which can be accessed free:

<http://www.sciencemag.org/content/345/6195/451.full.html#ref-list-1>

This article appears in the following **subject collections**:

Paleontology

<http://www.sciencemag.org/cgi/collection/paleo>

propagate away from the wells and disturbs a larger and larger volume, the probability increases that fluid pressure will encounter a larger fault and induce a larger-magnitude earthquake. The absence of earthquakes in regions above the critical pressure threshold may result from either a lack of faults or lack of well-oriented, critically stressed faults. Alternatively, fluid flow may preferentially migrate along bedding structure (Fig. 2A).

Though seven earthquakes were recorded in 2006 to 2009 near the base of the SE OK wellbores (10), the main swarm began ~15 km to the northeast (fig. S9), despite the high modeled pressure perturbation near the wells. Earthquakes in 2009 primarily occurred, within location uncertainty, near injection wells or on the nearest known faults to the northeast of the wells (fig. S9). Focal mechanisms near the swarm onset indicate fault planes at orientations favorable to failure (19) (Fig. 2, inset B). Faults subparallel to the north-northwest-south-southeast-trending Nemaha fault would not be well oriented for failure in the regional ~N70E stress regime (25) and would require substantially larger pressure increase to fail. Recent earthquakes near the fault may be evidence for continued pressure increase. This 50-km-long segment of the Nemaha fault is capable of hosting a *M*7 earthquake based on earthquake scaling laws (20), and the fault zone continues for hundreds of kilometers. The increasing proximity of the earthquake swarm to the Nemaha fault presents a potential hazard for the Oklahoma City metropolitan area.

Our earthquake relocations and pore pressure models indicate that four high-rate disposal wells are capable of increasing pore pressure above the reported triggering threshold (21–23) throughout the Jones swarm and thus are capable of triggering ~20% of 2008 to 2013 central and eastern U.S. seismicity. Nearly 45% of this region's seismicity, and currently nearly $15 M > 3$ earthquakes per week, may be linked to disposal of fluids generated during Oklahoma dewatering and after hydraulic fracturing, as recent Oklahoma seismicity dominantly occurs within seismic swarms in the Arbuckle Group, Hunton Group, and Mississippi Lime dewatering plays. The injection-linked seismicity near Jones occurs up to 35 km away from the disposal wells, much further than previously considered in existing criteria for induced seismicity (13). Modern, very high-rate injection wells can therefore affect regional seismicity and increase seismic hazard. Regular measurements of reservoir pressure at a range of distances and azimuths from high-rate disposal wells could verify our model and potentially provide early indication of seismic vulnerability.

REFERENCES AND NOTES

- W. L. Ellsworth, *Science* **341**, 1225942 (2013).
- K. Keranen, H. Savage, G. Abers, E. Cochran, *Geology* **41**, 699–702 (2013).
- W.-Y., *J. Geophys. Res.* **118**, 3506–3518 (2013).
- S. Horton, *Seismol. Res. Lett.* **83**, 250–260 (2012).
- C. Frohlich, C. Hayward, B. Stump, E. Potter, *Bull. Seismol. Soc. Am.* **101**, 327–340 (2011).
- A. H. Justinic, B. Stump, C. Hayward, C. Frohlich, *Bull. Seismol. Soc. Am.* **103**, 3083–3093 (2013).
- C. Frohlich, *Proc. Natl. Acad. Sci. U.S.A.* **109**, 13934–13938 (2012).
- A. McGarr, *J. Geophys. Res.* **119**, 1008–1019 (2014).
- The Central and Eastern United States is considered the portion of the contiguous United States east of 109°W.
- ANSS catalog, United States Geological Survey, <http://earthquake.usgs.gov/earthquakes/search/>, accessed 4/1/2014.
- N. J. van der Elst, H. M. Savage, K. M. Keranen, G. A. Abers, *Science* **341**, 164–167 (2013).
- D. F. Sumy, E. S. Cochran, K. M. Keranen, M. Wei, G. A. Abers, *J. Geophys. Res.* **119**, 1904–1923 (2014).
- S. D. Davis, C. Frohlich, *Seismol. Res. Lett.* **64**, 207–224 (1993).
- Information on materials and methods is available on Science Online.
- Oklahoma Corporation Commission Imaging Web Application, <http://imaging.occeweb.com/>
- D. Chernicky, *World Oil* (2000); www.worldoil.com/September-2000-Major-reserve-increase-obtained-by-dewatering-high-water-saturation-reservoirs.html.
- K. E. Murray, *Environ. Sci. Technol.* **47**, 4918–4925 (2013).
- F. Waldhauser, W. L. Ellsworth, *Bull. Seismol. Soc. Am.* **90**, 1353–1368 (2000).
- A. A. Holland, *Seismol. Res. Lett.* **84**, 876–890 (2013).
- D. L. Wells, K. J. Coppersmith, *Bull. Seismol. Soc. Am.* **84**, 974–1002 (1994).
- P. A. Reasenber, R. W. Simpson, *Science* **255**, 1687–1690 (1992).
- L. Seeber, J. G. Armbruster, *Nature* **407**, 69–72 (2000).
- R. Stein, *Nature* **402**, 605–609 (1999).
- M. D. Zoback, J. Townend, B. Grollimund, *Int. Geol. Rev.* **44**, 383–401 (2002).
- M. L. Zoback, *J. Geophys. Res.* **97**, 11703–11728 (1992).
- K. V. Luza, J. E. Lawson, *Oklahoma Geological Survey Spec. Pub.* **81-3**, 1–67 (1981).
- S. P. Gay, *Shale Shaker* **54**, 39–49 (2003).
- L. E. Gatewood, in *Geology of Giant Petroleum Fields*, AAPG Memoir **14**, M. T. Halbouty, Ed. (American Association of Petroleum Geologists Tulsa, OK, 1970).
- Monthly average volume was calculated by using reported volumes for any month with nonzero volume in data available from 1995 through 2012 (15). Injection rates over 90% larger than the median monthly value in a given year for each well were removed from calculations to remove data entry errors.

ACKNOWLEDGMENTS

This research benefited from discussion with E. Cochran, W. Ellsworth, and participants in a U.S. Geological Survey (USGS) Powell Center Working Group on Understanding Fluid Injection Induced Seismicity (M.W., B.A.B., and S.G. are part of this group). C. Hogan identified many P and S phases. K.M.K. was partially supported by USGS National Earthquake Hazards Reduction Program (NEHRP) grant G13AP00025, M.W. was partially supported by the USGS Powell Center grant G13AC00023, and G.A.A. was partially supported by NEHRP grant G13AP00024. This project used seismic data from EarthScope's Transportable Array, a facility funded by the National Science Foundation. Seismic waveforms are from the Incorporated Research Institutions for Seismology Data Management Center and the USGS CWB Query. Well data are from the Oklahoma Corporation Commission and the Oklahoma Geological Survey. Lists of wells and the local earthquake catalog are available as supplementary materials on Science Online.

SUPPLEMENTARY MATERIALS

www.sciencemag.org/content/345/6195/448/suppl/DC1
Materials and Methods
Figs. S1 to S10
Tables S1 to S9
References (30–41)

8 May 2014; accepted 24 June 2014

Published online 3 July 2014;

10.1126/science.1255802

DINOSAUR EVOLUTION

A Jurassic ornithischian dinosaur from Siberia with both feathers and scales

Pascal Godefroit,^{1*} Sofia M. Sinitsa,² Danielle Dhouailly,³ Yuri L. Bolotsky,⁴ Alexander V. Sizov,⁵ Maria E. McNamara,^{6,7} Michael J. Benton,⁷ Paul Spagna¹

Middle Jurassic to Early Cretaceous deposits from northeastern China have yielded varied theropod dinosaurs bearing feathers. Filamentous integumentary structures have also been described in ornithischian dinosaurs, but whether these filaments can be regarded as part of the evolutionary lineage toward feathers remains controversial. Here we describe a new basal neornithischian dinosaur from the Jurassic of Siberia with small scales around the distal hindlimb, larger imbricated scales around the tail, monofilaments around the head and the thorax, and more complex featherlike structures around the humerus, the femur, and the tibia. The discovery of these branched integumentary structures outside theropods suggests that featherlike structures coexisted with scales and were potentially widespread among the entire dinosaur clade; feathers may thus have been present in the earliest dinosaurs.

The origin of birds is one of the most-studied diversification events in the history of life. Principal debates relate to the origin of key avian features such as wings, feathers, and flight (1–9). Numerous finds from China have revealed that diverse theropods possessed feathers and various degrees of flight capability (4–9). The identification of melanosomes in non-avian theropods (10, 11) confirms that fully birdlike feathers originated within Theropoda at least 50 million years before *Archaeopteryx*.

But were feathers more widespread among dinosaurs? Quill-like structures have been reported in the ornithischians *Psittacosaurus* (12) and *Tianyulong* (13), but whether these were true feathers, or some other epidermal appendage, is

unclear. Bristlelike epidermal appendages occur in pterosaurs, some early theropods (14), and extant mammals (“hairs”), and so the *Psittacosaurus*

¹Directorate ‘Earth and History of Life,’ Royal Belgian Institute of Natural Sciences, Rue Vautier 29, B-1000 Brussels, Belgium. ²Institute of Natural Resources, Ecology and Cryology, 26 Butin Street, 672 014 Chita, Russia. ³UJF-CNRS FRE 3405, AGIM, Université Joseph Fourier, Site Santé, 38 706 La Tronche, France. ⁴Institute of Geology and Nature Management, FEB RAS, 1 Relochny Street 675 000, Blagoveshchensk, Russia. ⁵Institute of the Earth Crust, SB RAS, 128 Lermonov Street, Irkutsk, 664 033 Irkutsk, Russia. ⁶School of Biological, Earth and Environmental Science, University College Cork, Cork, Ireland. ⁷School of Earth Sciences, University of Bristol, Bristol BS8 1RJ, UK. *Corresponding author. E-mail: pascal.godefroit@naturalsciences.be

characters (Fig. 1, and figs. S4 to S7): maxilla with rostral ascending process much lower than caudal ascending process and maxillary fenestra larger than antorbital fenestra; jugal with notched postorbital ramus; postorbital with dorsoventrally expanded caudal ramus; dorsoventrally slender postacetabular process on ilium; and deep extensor fossae on metatarsals II to IV (15).

It was a small, 1.5-m-long bipedal herbivore, with a short skull, plant-eating teeth, elongate hindlimbs, short forelimbs, and an elongate tail (Fig. 1). Phylogenetic analysis (figs. S10 and S11) (15) recovers *Kulindadromeus* as a basal member of Neornithischia [all genasaurians more closely related to *Parasaurolophus walkeri* than to *Ankylosaurus magniventris* or *Stegosaurus stenops* (16)] and the sister taxon for Cerapoda [*Parasaurolophus walkeri*, *Triceratops horridus*, their most recent common ancestor, and all descendants (16)].

The key features of *Kulindadromeus* relate to its integument. Numerous, varied, exceptionally preserved integumentary features are associated, often in direct connection, with the bones and vary in morphology among different body regions. They comprise three types of scales and three types of featherlike structures.

Small (<3.5 mm long) imbricated and hexagonal scales, resembling the scutella in modern birds (17), are associated with the distal parts of the tibiae in *Kulindadromeus* (Fig. 2A and fig. S8E). Smaller (<1 mm) rounded and non-overlapping scales occur around the manus, tarsus (Fig. 2A and fig. S8E), metatarsus, and pes (fig. S8F), resembling the reticula along the plantar face of the pes in modern birds (17). The tail of *Kulindadromeus* is covered by at least five longitudinal rows of slightly arched scales (Fig. 2, B and C, and fig. S8, A to D). The largest scales (~20 mm long and 10 mm wide) occur along the proximal part of the tail. The caudal scales of *Kulindadromeus* are thin (<100 μm), unornamented, and slightly imbricated, each scale covering part of the adjacent distal one (Fig. 2C and fig. S8, B to D). They are clearly different from the thicker, sculptured, and nonoverlapping osteoderms in thyreophoran ornithischians (18) and from the proportionally thicker and smaller scales in iguanodontian ornithopods (19), more closely resembling epidermal scales. The preservation of the scales as carbonaceous remains suggests that they are unlikely to be osteoderms, because the bones

(which also comprise calcium phosphate in vivo) display a quite different preservational pathway. Each scale forms a triangular anterior spur that covers the preceding one, so that adjacent elements are interconnected by a clip-like system. Proximally, at the level of the base of the tail (Fig. 2C), the scales become progressively smaller and more rounded and do not overlap.

Monofilaments are widely distributed around the thorax (Fig. 2, G to I), on the back, and around the head (Fig. 2, D to F). Those above the head are thin (~0.15 mm in diameter), short (10 to 15 mm long), and curved, with no preferred orientation. The thoracic and abdominal filaments are wider (0.2 to 0.3 mm) and longer (20 to 30 mm). These monofilaments are shorter and thinner than the long bristlelike structures on the proximal part of the tail in *Psittacosaurus* (12) and the filamentous structures in *Tiamyulong* (13). They more closely resemble the monofilaments in the basal coelurosaur *Sinosauropteryx* (20) and are similar to morphotype 1 in a recent evolutionary model of feathers (21).

Kulindadromeus also shows compound, non-shafted integumentary structures along the humerus and femur (Fig. 3, A to F, and fig. S9).

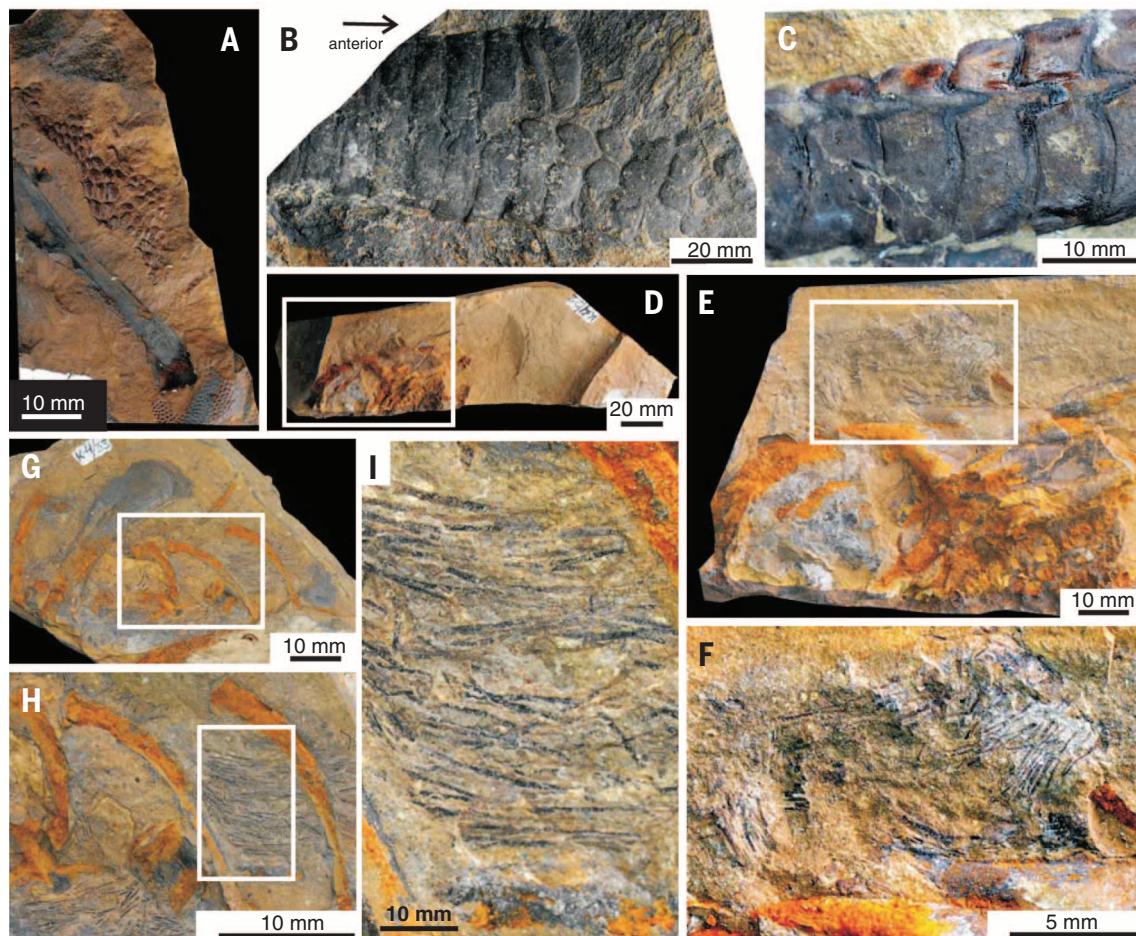


Fig. 2. Epidermal scales and featherlike structures of *Kulindadromeus zabaikalicus*. (A) Scales around the distal tibia and the tarsus (INREC K4/57); (B) double row of scales above the proximal part of the tail (INREC K4/94) in dorsal view; (C) close-up of the left row of caudal scales (INREC K4/117) in dorsal view; (D) partial skull (INREC K4/22) in right lateral view, with (E and F) detail of areas indicated in (D) and (E) showing filamentous structures; (G) left part of ribcage (INREC K4/33), with (H and I) detail of areas indicated in (G) and (H) showing filamentous structures.

These occur as groups of six or seven filaments that converge proximally and arise from the central regions of a basal plate. Individual filaments are 10 to 15 mm long. Those on the humerus are wider (0.2 to 0.4 mm) and straighter than those on the femur (0.1 to 0.2 mm). These groups of filaments are similar to feather morphotype 3 (21, 22) and resemble the down feathers of some modern chicken breeds, such as the Silkie, which are devoid of barbules (17). The basal plates are also larger on the humerus (3 to 4 mm wide) than on the femur (2 to 3 mm); they are arranged in a hexagonal pattern, but

they remain distinctly separated from each other, contrasting with the contiguous distribution of the scales on the distal forelimb, hindlimb, and tail in *Kulindadromeus* and also with the feathered scales that cover the tarsometatarsus of some living birds (17). Whether the basal plates represent modified scales or calamus-like structures remains unclear and requires further investigation.

An additional integumentary morphotype occurs along the proximal part of the tibia in *Kulindadromeus* (Fig. 3, G to J): Clusters of six or seven ribbon-shaped elements appear more or

less bundled together proximally, close to the bone surface. Each individual element is 15 to 20 mm long and 1.5 to 3 mm wide, with a dark median axis along its length (Fig. 3, H to J). Careful removal of a thin superficial carbonaceous sheet reveals the presence of ~10 thin (50 to 100 μm) internal parallel filaments within each ribbon-shaped element (Fig. 3J). This is an arrangement that has never previously been reported and that could represent a third feather-like morphotype in *Kulindadromeus*.

The presence of both simple and compound filamentous structures in *Kulindadromeus*

Fig. 3. Featherlike structures in *Kulindadromeus zabaikalicus*. (A) Right humerus and proximal part of right radius and ulna (INREC K4/115), with detail (B) and interpretative drawing (C) of compound structures around the right humerus; (D and E) compound structures around femur (counterpart of INREC K4/116) with (F) interpretative drawing of (E); (G) ribbonlike structures around proximal part of tibia (INREC K4/44); the inset shows the slab at lower magnification. (H) Detail of area indicated in (G) with interpretative drawing (I) and further details of ribbonlike structures (J); the superficial carbonaceous sheet has been removed during preparation, revealing an internal structure of thin parallel filaments (red arrow). Abbreviation: bpl, basal plate.

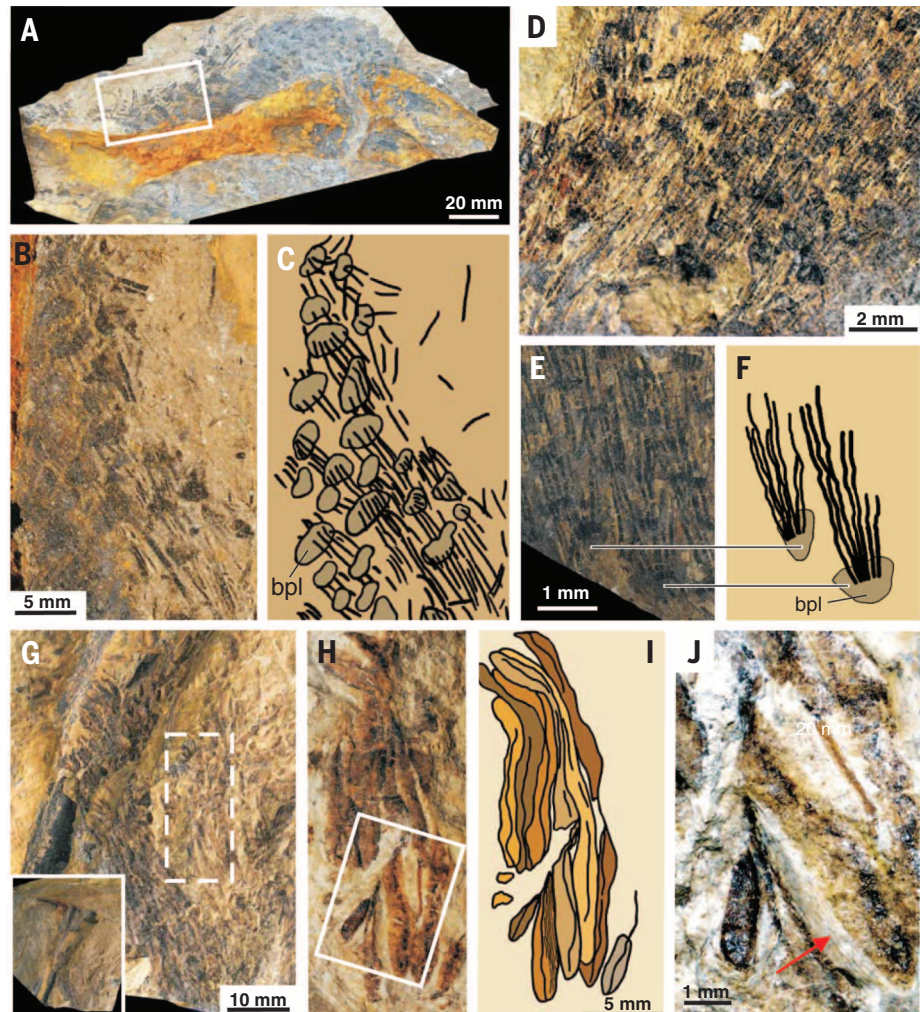
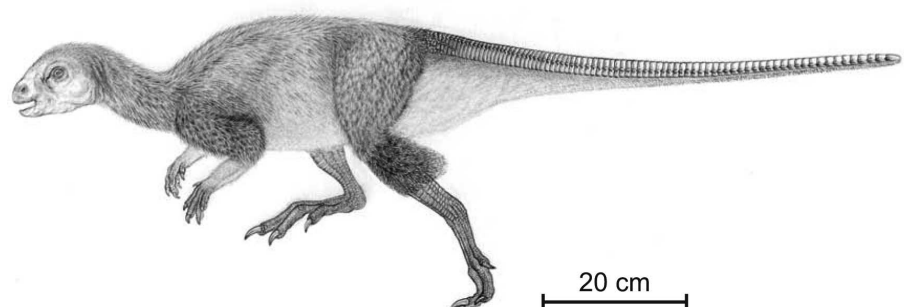


Fig. 4. Reconstruction of *Kulindadromeus zabaikalicus*. A basal ornithomimid dinosaur, with feathers and scales, from the Middle to Late Jurassic of southeastern Siberia. [Drawing by Pascale Golinvaux (Royal Belgian Institute of Natural Sciences)]



(Fig. 4) supports the hypothesis that the integumentary structures in Ornithischia, already described in *Psittacosaurus* (12) and *Tianyulong* (13), could be homologous to the “protofeathers” in non-avian theropods. In any case, it indicates that those protofeather-like structures were probably widespread in Dinosauria, possibly even in the earliest members of the clade. Further, the ability to form simple monofilaments and more complex compound structures is potentially nested within the archosauromorph clade, as exemplified by *Longisquama* (23), pterosaurs (24), ornithischians, and theropods (including birds).

In *Kulindadromeus* and most ornithuromorph birds (17, 25), the distal hindlimb is extensively covered by scales and devoid of featherlike structures. This condition might thus be primitive in dinosaurs. Both paleontological and genetic evidence, however, suggests that the pedal scales of ornithuromorph birds are secondarily derived from feathers. In avialan evolution, leg feathers were reduced gradually in a distal-to-proximal direction, with eventual loss of the distal feathers and appearance of pedal scales in ornithuromorphs (25). Further, evo-devo experiments (26, 27) show that feathers in extant birds are the default fate of the avian epidermis, and that the formation of avian scales requires the inhibition of feather development. The local formation of scales requires the inhibition of epidermal outgrowth, regulated by the *sonic hedgehog* pathway; this inhibition is partially lost in the case of breeds with feathered feet (27). Therefore, it is possible that the extensively scaled distal hindlimbs in *Kulindadromeus* might be explained by similar local and partial inhibition in the development of featherlike structures. The preservation of featherlike structures and scales in the basal neornithischian *Kulindadromeus*, and their similarity to structures that are present in diverse theropods and ornithuromorph birds, thus strongly suggest that deep homology mechanisms (28) explain the complex distribution of skin appendages within dinosaurs (23).

REFERENCES AND NOTES

- M. A. Norell, X. Xu, *Annu. Rev. Earth Planet. Sci.* **33**, 277–299 (2005).
- T. Lingham-Soliar, A. Feduccia, X. Wang, *Proc. Biol. Sci.* **274**, 2823 (2007).
- F. Zhang, Z. Zhou, G. Dyke, *Geol. J.* **41**, 395 (2006).
- T. Lingham-Soliar, *Proc. Biol. Sci.* **275**, 775–780 (2008).
- D. Hu, L. Hou, L. Zhang, X. Xu, *Nature* **461**, 640–643 (2009).
- S. L. Brusatte *et al.*, *Earth Sci. Rev.* **101**, 68–100 (2010).
- X. Xu, H. You, K. Du, F. Han, *Nature* **475**, 465–470 (2011).
- P. Godefroit *et al.*, *Nat. Commun.* **4**, 1394 (2013).
- P. Godefroit *et al.*, *Nature* **498**, 359–362 (2013).
- F. Zhang *et al.*, *Nature* **463**, 1075–1078 (2010).
- Q. Li *et al.*, *Science* **327**, 1369–1372 (2010).
- G. Mayr, D. S. Peters, G. Plodowski, O. Vogel, *Naturwissenschaften* **89**, 361–365 (2002).
- X.-T. Zheng, H.-L. You, X. Xu, Z.-M. Dong, *Nature* **458**, 333–336 (2009).
- O. W. M. Rauhut, C. Foth, H. Tischlinger, M. A. Norell, *Proc. Natl. Acad. Sci. U.S.A.* **109**, 11746–11751 (2012).
- See the supplementary materials on Science Online.
- R. J. Butler, P. Upchurch, D. B. Norman, *J. Syst. Palaeontology* **6**, 1–40 (2008).
- A. M. Lucas, P. R. Stettenheim, *Avian Anatomy, Integument* (U.S. Department of Agriculture, Washington, DC, 1972).

- M. K. Vickarous, T. Maryanska, D. B. Weishampel, in *The Dinosauria 2nd edn.*, D. B. Weishampel, P. Dodson, H. Osmolska, Eds. (Univ. of California Press, Berkeley, CA, 2004), pp. 363–392.
- P. R. Bell, *PLOS ONE* **7**, e31295 (2012).
- P. J. Currie, P. J. Chen, *Can. J. Earth Sci.* **38**, 1705–1727 (2001).
- X. Xu, X. Zheng, H. You, *Nature* **464**, 1338–1341 (2010).
- F. Zhang, Z. Zhou, X. Xu, X. Wang, C. Sullivan, *Nature* **455**, 1105–1108 (2008).
- M. Buchwitz, S. Voigt, *Paläontol. Z.* **86**, 313 (2012).
- X. Wang, Z. Zhou, F. Zhang, X. Xu, *Chin. Sci. Bull.* **47**, 226 (2002).
- X. Zheng *et al.*, *Science* **339**, 1309–1312 (2013).
- D. Dhouailly, *J. Anat.* **214**, 587–606 (2009).
- F. Prin, D. Dhouailly, *Int. J. Dev. Biol.* **48**, 137–148 (2004).
- N. Shubin, C. Tabin, S. Carroll, *Nature* **388**, 639–648 (1997).

ACKNOWLEDGMENTS

We thank A. B. Ptitsyn for making fossils available for study; Ph. Claeys, J.-M. Baele, and I. Y. Bolosky for help and comments on the manuscript; and P. Golinvaux, J. Dos Remedios Esteves, C. Desmedt, and A. Vandersypen for the drawings and reconstructions. This study was supported by Belgian Science Policy grant BL/36/62 to P.G. and by Natural Environment Research Council Standard Grant NE/1027630/1 awarded to M.J.B.

SUPPLEMENTARY MATERIALS

www.sciencemag.org/content/345/6195/451/suppl/DC1
Materials and Methods
Supplementary Text
Figs. S1 to S11
References (29–55)

13 March 2014; accepted 23 June 2014
10.1126/science.1253351

RNA FUNCTION

Ribosome stalling induced by mutation of a CNS-specific tRNA causes neurodegeneration

Ryuta Ishimura,^{1*} Gabor Nagy,^{1*} Ivan Dotu,² Huihao Zhou,³ Xiang-Lei Yang,³ Paul Schimmel,³ Satoru Senju,⁴ Yasuharu Nishimura,⁴ Jeffrey H. Chuang,² Susan L. Ackerman^{1†}

In higher eukaryotes, transfer RNAs (tRNAs) with the same anticodon are encoded by multiple nuclear genes, and little is known about how mutations in these genes affect translation and cellular homeostasis. Similarly, the surveillance systems that respond to such defects in higher eukaryotes are not clear. Here, we discover that loss of GTPBP2, a novel binding partner of the ribosome recycling protein Pelota, in mice with a mutation in a tRNA gene that is specifically expressed in the central nervous system causes ribosome stalling and widespread neurodegeneration. Our results not only define GTPBP2 as a ribosome rescue factor but also unmask the disease potential of mutations in nuclear-encoded tRNA genes.

In higher eukaryotes, the nuclear genome typically contains several hundred transfer RNA (tRNA) genes, which fall into isoacceptor groups, each representing an anticodon (1). Relative to the total number of tRNA genes, the number of isodecoders—i.e., tRNA molecules with the same anticodon but differences in the tRNA body—increases dramatically with organismal complexity, which leads to speculation that isodecoders might not be fully redundant with one another (2). Overexpression of reporter constructs with rare codons that are decoded by correspondingly low-abundance tRNAs in bacteria and yeast, or mutations in single-copy

mitochondrial tRNA genes, may result in stalled elongation complexes (3–5). However, the consequences of mutations in multicopy, nuclear-encoded tRNA isodecoder genes or in the surveillance systems that eliminate the effect of such tRNA mutations are not known in higher eukaryotes.

The *nmf205* mutation was identified in an *N-ethyl-N-nitrosourea* mutagenesis screen of C57BL/6J (B6J) mice for neurological phenotypes (6). B6J-*nmf205*^{-/-} mice were indistinguishable from wild-type mice at 3 weeks of age but showed clear truncal ataxia at 6 weeks (movie S1). Mice died at 8 to 9 weeks with severe locomotor deficits. Progressive apoptosis of neurons in the inner granule layer (IGL) in the mutant cerebellum was initially observed between 3 and 4 weeks of age (Fig. 1, A to H). Apoptosis of mutant granule cells in the dentate gyrus, CA2 pyramidal neurons, and layer IV cortical neurons occurred between 5 and 8 weeks of age (Fig. 1, I and J, and fig. S1, A to H). Further, many neurons in the retina—including photoreceptors and amacrine, horizontal, and ganglion cells—degenerated during this time (Fig. 1, K and L, and fig. S1, I to T).

¹Howard Hughes Medical Institute and The Jackson Laboratory, 600 Main Street, Bar Harbor, ME 04609, USA. ²The Jackson Laboratory for Genomic Medicine, 263 Farmington Avenue, Farmington, CT 06030, USA. ³The Skaggs Institute for Chemical Biology, The Scripps Research Institute, 10550 North Torrey Pines Road, La Jolla, CA 92037, USA. ⁴Department of Immunogenetics, Graduate School of Medical Sciences, Kumamoto University, Honjo 1-1-1, Chuo-ku, Kumamoto 860-8556, Japan.

*These authors contributed equally to this work. †Corresponding author. E-mail: susan.ackerman@jax.org